Improving 3D-printed high-impact polystyrene using fused filament fabrication via multi-objective optimisation

Phan Quoc Khang Nguyen, Y.X. Zhang, Zhongpu Zhang and Richard (Chunhui) Yang
Centre for Advanced Manufacturing Technology, School of Engineering, Design and Built Environment, Western Sydney University, Sydney, Australia

Abstract

Purpose – This study aims to improve mechanical strength and build time of Fused Filament Fabrication (FFF)-printed high-impact polystyrene (HIPS), considering five key controllable FFF process parameters including layer thickness, printing speed, number of contours, raster angle and infill density and their effects on mechanical performance of the HIPS.

Design/methodology/approach – This study develops a novel multistage material optimisation framework with a mixing experimental and theoretical analysis procedures for FFF of thermoplastic polymers. Artificial neuron network (ANN) is adopted for pattern recognition before the genetic algorithm (GA) and multi-criteria decision-making algorithm are applied for optimisation.

Findings – Optimised FFF-printing HIPS with rational balance between mechanical properties (tensile strength, flexural strength and impact strength) and build time were achieved. The infill density as the main contributor to the tensile strength and flexural strength, the raster angle as the main contributor to the impact strength while the layer thickness has the highest impact on the build time. ANN-GA method succeeds at achieving a reasonable balance of mechanical strength and build time.

Originality/value – User-friendly and innovative methodology are devised for developing highly accurate ANN-GA-TOPSIS models for multi-objective optimisation. Optimum settings for three-dimensional-printing HIPS with rational balance between mechanical properties (tensile strength, flexural strength and impact strength) and build time are achieved. The outcome of this research can be useful to achieve high-performance FFF-printed HIPS parts for automotive industries and medical fields with significantly reduced build time.

Keywords Fused filament fabrication (FFF), Multi-objective optimisation, Mechanical properties, Build time, Machine learning, High-impact polystyrene (HIPS)

Paper type Research paper

1. Introduction

Additive manufacturing (AM), also referred to three-dimensional (3D) printing, stands at the forefront of advanced manufacturing technologies, revolutionising traditional manufacturing methods. This innovative process builds 3D objects layer by layer, offering unparalleled design flexibility, reduced material waste and the capacity to create intricate and complex structures, marking a paradigm shift in manufacturing efficiency and customisation (Alarifi, 2023; Almutairi *et al.*, 2023). AM has emerged as a transformative technology with diverse applications, revolutionising the aerospace industry through lightweight and intricately designed components, enhancing medical practices with customised implants and prosthetics (Bregoli *et al.*, 2024) and reshaping the construction sector by enabling the on-site production of complex and tailored building components (Ngo *et al.*, 2018; Shemelya *et al.*, 2017).

Among the various AM techniques, Fused Filament Fabrication (FFF) is the most prominent one and has been widely used in various industries for rapid prototyping, functional part production and educational purposes. However, optimisation of FFF process parameters is crucial for achieving consistent and high-quality FFF-printed objects, which can fulfil the requirements on mechanical strength, surface roughness and dimensional accuracy (Zohdi and Yang, 2021). In literature, flexural strength (FS) and yield strength of FFF-printed acrylonitrile butadiene styrene (ABS) under the variation of layer thickness, nozzle diameter, infill density, printing speed, raster angle and infill pattern were optimised using artificial neural network (ANN) and genetic algorithm (GA) (Tayyab *et al.*, 2023). Samykano *et al.* (2019) investigated the effects of three FFF process parameters including layer

The current issue and full text archive of this journal is available on Emerald Insight at: **https://www.emerald.com/insight/1355-2546.htm**

Rapid Prototyping Journal
31/11 (2025) 284–300
Emerald Publishing Limited [ISSN 1355-2546]
[DOI 10.1108/RPJ-01-2025-0028]

Competing interest: No potential competing interest was reported by the authors.

Received 2 February 2025
Revised 6 April 2025
28 June 2025
Accepted 18 August 2025

thickness, infill density and raster angle on the tensile strength (TS), elastic modulus and yield strength of FFF-printed ABS. They concluded that the infill density was the most influential factor. Singh *et al.* (2019) printed ABS/high-impact polystyrene (HIPS) multi-material samples to study the effects of five process parameters – layer thickness, infill density, number of contours, raster angles and number of solid layers on their material properties, including TS, impact strength (IS) and FS. In a different study (Kumar *et al.*, 2022), the effects of layer thickness, extrusion temperature, printing speed and raster width were investigated to optimise the surface roughness (SR), build time (BT) and volume percentage error (VPE). The analysis and optimisation were performed using ANN and the whale optimisation algorithm. The layer thickness was concluded to be the most significant factor for SR, BT and VPE. In another literature (Cerro *et al.*, 2021), multiple machine learning models were evaluated to study the non-linearity effects of layer thickness, printing speed, number of contours, build orientation and extrusion temperature on the surface roughness using polyvinyl butyral. Layer thickness and build orientation were found to have the highest impact on the surface roughness. Although the FFF process parameters' effects on material properties of FFF-printed materials has been extensively investigated, most studies only concentrated on common feedstock materials for FFF such as ABS and polylactic acid (PLA) (Dey and Yodo, 2019). Hence, current literature elicit a need for adopting other materials such as HIPS, which are commonly used for automotive industries (Romero *et al.*, 2021), pharmaceutical applications (Pires *et al.*, 2020) and medical applications (Pinho *et al.*, 2021).

Multi-objective optimisation in FFF holds a distinct advantage over single-objective optimisation by considering a broader range of factors simultaneously. While single-objective optimisation may focus solely on one aspect, such as TS or material usage, multi-objective optimisation balances multiple factors like material strength, surface finish and time efficiency. This holistic approach results in more well-rounded solutions that cater to real-world complexities and trade-offs, leading to 3D-printed parts that excel across various criteria and better align with complex design requirements and manufacturing constraints. Gurrala and Regalla (2014) performed multi-objective optimisation for the TS and volume shrinkage of FFF-printed parts by controlling the model interior, horizontal direction and vertical direction. Non-dominated sorting genetic algorithm II (NSGA-II) was deployed to maximise the TS and minimise volume shrinkage. In another study (Raju *et al.*, 2019), the experiment was planned based on the Taguchi array to examine the effects of layer thickness, support material, model interior and orientation and perform multi-objective optimisation for hardness, TS, flexural modulus and surface quality. All the responses were merged with suitable weight into a single response for optimisation using particle swarm optimisation (PSO), bacterial foraging optimisation (BFO) and hybrid PSO–BFO. Anand *et al.* (2025) aimed to maximise the tensile and FS of FFF-printed polyethylene terephthalate glycol (PETG) parts and the results revealed infill density and layer thickness as the most influential factors. The authors also nominated hybrid PSO–BFO for multi-objective optimisation. In a different study, multi-objective optimisation was carried out to optimise arithmetic roughness, profile irregularity, asymmetry and surface flattening of FFF-printed PLA parts using response surface methodology (Ben Rezg *et al.*, 2025). Apart from addressing part qualities, multi-objective optimisation was also deployed to produce FFF-printed wheel spindle in combination with topological optimisation (Asadollahi-Yazdi *et al.*, 2019).

The technique for order of preference by similarity to ideal solution (TOPSIS) is a decision-making method used to evaluate and rank a set of alternatives based on multiple criteria. In the context of FFF, TOPSIS holds importance as it enables a systematic approach to assess and select optimal combinations of process parameters for 3D printing. By considering various factors such as surface finish, mechanical properties, material usage and printing time, TOPSIS aids in identifying the most suitable parameter settings that strike a balance between competing objectives. In a study by Dev and Srivastava (2023), TOPSIS was applied to execute the multi-objective optimisation for TS, FS and material weight (MW). The experiment was planned based on central composite design and the controlled process parameters are layer thickness, raster angle, extrusion temperature, printing speed and infill density. Analysis of variance (ANOVA) results indicated the infill density as the highest influential factor for all responses. The sequential results of ANN-GA-TOPSIS were found to improve the TS, FS and MW by 6.45%, 4.19% and 11.47%. In another study (Kamaal *et al.*, 2021), the TOPSIS was used to determine the optimal process parameters for TS and IS when the materials were printed under the variation of layer thickness, infill density and build orientation, and results also revealed the increase of FS relative to the increase in layer thickness and infill density. After the RSM-NSGII generated a family of optimal solutions, TOPSIS was deployed to rank the solutions to optimise the BT, MW and compressive strength of FFF-printed PLA parts (Dixit *et al.*, 2024). TOPSIS was also integrated with grey world optimiser to maximise energy consumption and part quality of FFF-printed parts (Yan *et al.*, 2025).

In the preliminary study conducted by the authors (Zohdi and Yang, 2019), FFF-printed HIPS samples demonstrated a lower degree of anisotropy when printed at longitudinal and transverse build orientation compared to their FFF-printed ABS counterparts. In addition, despite of the aforementioned unique characteristic and its significant applications in the composites manufacturing (Sieradzka *et al.*, 2021; Thuong *et al.*, 2024; Zaafarani *et al.*, 2024), automotive (Romero *et al.*, 2021) and medical (Pires *et al.*, 2020; Xu *et al.*, 2018; Pinho *et al.*, 2021) fields, HIPS has not been extensively researched. Current landscape of the FFF technique is showing an absence of dedicated multi-objective optimisation, especially for uncommon FFF-printed materials such as HIPS. In addition, the current research lacks comprehensive exploration into the impacts of key FFF process parameters on all three fundamental strengths of thermoplastic polymers –TS, FS and IS – restricting a holistic understanding of the interplay between fabrication variables and mechanical performance. Moreover, the existing literatures predominantly emphasised the optimisation of mechanical strength in FFF but overlooked the crucial factor of BT and thereby neglected a vital dimension of efficiency in the manufacturing workflow.

To fill the identified research gaps, the first objective of this study is to develop a novel multistage material optimisation

framework with mixing experimental and theoretical analysis procedures for FFF of thermoplastic polymers. FFF-printed HIPS is selected as the candidate material for research and testing. The second objective is to understand the effects of five key FFF process parameters, including layer thickness, printing speed, number of contours, raster angle and infill density, on the TS, FS and IS of FFF-printed HIPS. After these, for the first time, multi-objective optimisation is performed to strike the balance between three mechanical strengths and BT of FFF-printed HIPS via developing an ANN-GA-TOPSIS optimisation model, which is the third objective of this study.

This paper is outlined in the following main sections: Section 2 develops an four-stage material optimisation framework and experimental, mathematical analysis and optimisation procedures for FFF-printed HIPS; Section 3 presents the obtained results of FFF-printed HIPS and conducts technical discussions to reveal the effects of key FFF process parameters on their material properties; Section 4 presents the outcomes of the devised multi-objective optimisation, which are validated by those obtained experimental data; Section 5 further analyses the fracture surfaces of FFF-printed samples via scanning electron microscopy (SEM) analysis; and Section 6 draws conclusions for the research and oversees the future work.

2. Materials and methods

2.1 Development of four-stage material optimisation framework for FFF-printed HIPS

In this study, a four-stage-integrated experimental and theoretical analysis and optimisation framework for optimising FFF-printed HIPS is developed as depicted in Figure 1. In Stage 1, a Taguchi L27 array was used to collect data on the TS, FS, IS and BT of FFF-printed HIPS samples. This data set, comprising 27 data points, was then used in Stage 2 to train the ANN models, with a distinct predictive model developed for each response variable. In Stage 3, GA and TOPSIS were applied to the predictive models to generate optimal solutions. The main objectives were to maximise TS, FS and IS while minimising BT. Stage 4 involved additional experimental work to validate the predictive models. The effectiveness of the ANN-GA-TOPSIS models was assessed by comparing their predictions with experimental results. In addition, the experimental values of the optimal parameter sets were compared to the maximum strength observed in the original data set. Ultimately, the optimal FFF process parameters were identified by balancing the reliability of the predictive models with the observed improvements.

2.2 Sample design and experimental procedure

This study adopted three ASTM standards including ASTM-D638, ASTM-D790 and ASTM-D6110 for tensile, flexural and Charpy impact testings, respectively. The 3D models of testing specimens were designed using SolidWorks, sliced in Flash Print 5 before being imported into a Flashforge Creator 3 Pro for the 3D printing process. The printer was calibrated using the Flashforge Creator 3 Pro's built-in semi-automatic calibration method, which includes manual bed levelling and Z-offset calibration for each extruder to ensure proper first-layer adhesion and inter-nozzle alignment. The primary material used for the 3D printing process was HIPS with the following raw filament material properties as listed: a TS of 26 MPa, an FS of 40 MPa and an IS of 17 kJ/m^2 at 23°C, notched. The experimental design for this study was structured using the Taguchi L27 orthogonal array. The goal was to comprehensively analyse the effects of five key process parameters including layer thickness, printing speed, number of contours, raster angle and infill density. Taguchi L27 was selected because it allows the evaluation of three levels for each of the five process parameters using an orthogonal array, providing a balanced and efficient design with significantly fewer runs than a full factorial design (243 runs) while offering more interaction insight and resolution than an L9 design. Each factor was varied at three distinct levels as shown in Table 1 and then their ranges were suitably determined from printing trials. Other fixed parameters are also illustrated in Table 1. The ambient temperature was maintained at approximately 25°C. Because HIPS is sensitive to warping and delamination, printing was conducted in an enclosed chamber. Relative humidity was kept below 50%. To mitigate moisture absorption, the filament was stored in the dry chamber and pre-dried for 2–3 h before printing. In this context, as the cross angle was fixed at 90°, the raster angle of 22° indicated the first layer was created with a raster angle of 22° and the next layer would be generated by shifting the raster angle of previous layer by 90°.

Using the Taguchi array yielded a total of 27 distinct combinations of the five key process parameters. Each of these combinations, referred to as a "run", encapsulated a unique configuration of layer thickness, printing speed, number of contours, raster angle and infill density. Within each run, a batch of 5 specimens was fabricated for each of 3 mechanical properties, resulting in a total of 3 batches with 15 specimens used for mechanical testing purposes [see Figure 2 (a)–(c)]. The tensile process was conducted using the 5-kN Instron Machine with a strain rate of 1 mm/min. The three-point bending testing was performed on the same 5-kN Instron

Figure 1 Schematic of the developed systematic experimental and theoretical analysis framework for extracting material properties and optimisation

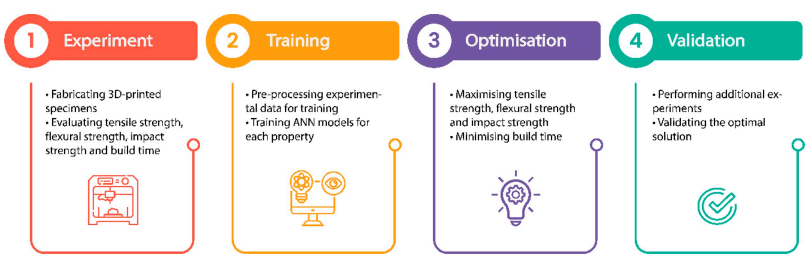

Source: Figure by authors

Table 1 Process parameters and their levels

Parameter	Notation	Units	No. of levels	Level 1	Level 2	Level 3
Layer thickness (LT)	X_1	mm	3	0.1	0.2	0.3
Printing speed (PS)	X_2	mm/s	3	40	70	100
Number of contours (NC)	X_3	–	3	1	2	3
Raster angle (RA)	X_4	°	3	0	22	45
Infill density (ID)	X_5	%	3	40	70	100
Build orientation	–	–	1	Longitudinal	–	–
Extrusion temperature	–	°C	1	230	–	–
Bed temperature	–	°C	1	110	–	–
Cross angle		°	1	90	–	–
Fan speed	–	%	1	15	–	–
Nozzle diameter	–	mm	1	0.4	–	–

Source(s): Table by authors

Figure 2 (a) One batch of tensile specimens for Run 16; (b) one batch of flexural specimens for Run 25; and (c) one batch of impact specimens for Run 12

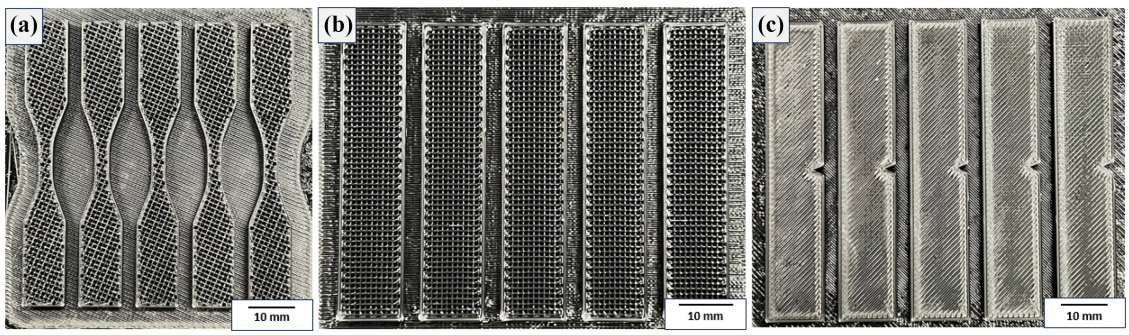

Source: Figure by authors

Machine with a strain rate of 10 mm/min. Meanwhile, the Charpy impact testing was conducted using the Instron CEAST9050 Pendulum Impact Testing Machine. The values presented in Table 2 for TS, FS and IS in each run represent the average across all specimens of that batch. Likewise, the BT listed in Table 2 for each run was calculated by dividing the total manufacturing time of all specimens by the total number of specimens in that run, representing the general BT for a single specimen encapsulating the geometries of all testing specimens.

From Table 2, Run 9 results in the optimum TS at 0.1 mm LT, 100 mm/s PS, 3 NC, 45°C RA and 100% ID. Maximum FS is found at Run 27 with 0.3 mm LT, 100 mm/s PS, 2 NC, 0°C RA and 100% ID. Meanwhile, setting 0.3 mm LT, 70 mm/s PS, 1 NC, 45°C RA and 100% ID for Run 24 maximises the IS while the minimum BT is attained at Run 25 with 0.3 mm LT, 100 mm/s PS, 2 NC, 0°C RA and 40% ID.

2.3 Artificial neural network model

ANNs have a profound ability to model complex, non-linear relationships between material properties and diverse process parameters. However, selecting the optimal ANN architecture often remains a labour-intensive, trial-and-error process guided by a researcher's expertise. For instance, Vijayaraghavan *et al.* (2015) experimented with ANN structures featuring hidden layers ranging from 1 to 4 and neurons between 2 and 9 per layer to identify the best-performing model. Similarly, Chinchanikar *et al.* (2022) explored configurations with up to three hidden layers and neuron counts spanning 10–750, achieving a correlation coefficient of 0.875 and an *R*-squared value of 0.765. Tayyab *et al.* (2023) optimised their ANN model for FS using two hidden layers and a Bayesian algorithm. Alafaghani *et al.* (2021) pushed this approach further by testing various combinations of hidden layers (1–2), neurons (3–10) and transfer functions, ultimately averaging the outputs of 36 models to refine predictions. In a different study, after setting the number of hidden layers to 1, Ali and Esakki (2020) optimised the neural network architecture and found that using seven neurons resulted in the lowest mean square error. While these manual optimisation techniques are suitable for relatively simple data sets or limited process parameters, they encounter significant scalability issues with more extensive or complex data sets. As an illustration, Tura *et al.* (2023) achieved an impressive correlation coefficient of 0.99 for TS predictions based on three process parameters and 15 experimental points. However, expanding the data set to 30 runs while maintaining the same number of parameters caused the *R* value to drop to 0.97 (Yadav *et al.*, 2020), underscoring the diminishing efficiency of manual model tuning in more demanding scenarios. These challenges point to the necessity of modernising the ANN optimisation process. Instead of relying solely on iterative trial-and-error approaches, integrating advanced software tools and automated

Table 2 Experimental design matrix and corresponding responses

Run	LT	PS	NC	RA	ID	Tensile strength (MPa)	Flexural strength (MPa)	Impact strength (kJ/m^2)	Build time (min)
1	0.1	40	1	0	40	6.8 ± 0.28	4.2 ± 0.24	3.9 ± 0.73	19.3
2	0.1	40	1	0	70	9.5 ± 0.30	14.4 ± 2.18	4.8 ± 0.74	26.9
3	0.1	40	1	0	100	19.6 ± 0.68	33.3 ± 2.22	7.4 ± 1.39	34.3
4	0.1	70	2	22	40	10.4 ± 0.20	7.6 ± 1.33	7.2 ± 1.22	18.7
5	0.1	70	2	22	70	13.3 ± 0.24	17.2 ± 0.99	6.1 ± 0.31	24.8
6	0.1	70	2	22	100	21.9 ± 0.50	28.1 ± 1.46	7.8 ± 0.69	30.8
7	0.1	100	3	45	40	13.7 ± 0.43	12.9 ± 1.60	9.2 ± 0.78	19.7
8	0.1	100	3	45	70	17.3 ± 0.54	14.4 ± 1.46	8.1 ± 0.59	25.6
9	0.1	100	3	45	100	24.0 ± 1.04	28.9 ± 1.95	10.0 ± 0.69	31.3
10	0.2	40	2	45	40	10.4 ± 0.28	8.2 ± 0.73	6.0 ± 0.69	13.3
11	0.2	40	2	45	70	13.6 ± 1.07	18.0 ± 2.51	10.2 ± 0.81	17.0
12	0.2	40	2	45	100	17.4 ± 0.99	33.0 ± 1.82	11.9 ± 1.00	20.7
13	0.2	70	3	0	40	15.2 ± 0.73	11.2 ± 0.46	6.5 ± 0.57	11.5
14	0.2	70	3	0	70	16.2 ± 0.56	19.2 ± 1.90	6.8 ± 0.42	14.3
15	0.2	70	3	0	100	19.7 ± 1.38	29.8 ± 2.19	6.2 ± 0.31	17.0
16	0.2	100	1	22	40	6.6 ± 0.42	8.6 ± 1.25	4.7 ± 0.62	10.5
17	0.2	100	1	22	70	8.1 ± 0.25	16.8 ± 1.61	5.5 ± 0.35	13.9
18	0.2	100	1	22	100	19.6 ± 0.97	32.5 ± 1.36	6.0 ± 0.19	17.2
19	0.3	40	3	22	40	14.4 ± 0.27	13.6 ± 1.47	7.8 ± 0.61	11.0
20	0.3	40	3	22	70	16.6 ± 0.30	17.8 ± 1.43	6.5 ± 0.51	13.3
21	0.3	40	3	22	100	19.1 ± 0.53	32.0 ± 1.75	8.7 ± 0.67	15.5
22	0.3	70	1	45	40	6.5 ± 0.10	6.7 ± 0.63	11.6 ± 2.37	8.5
23	0.3	70	1	45	70	8.7 ± 0.27	13.1 ± 0.53	11.4 ± 0.31	11.0
24	0.3	70	1	45	100	18.1 ± 0.84	32.2 ± 1.32	13.4 ± 0.88	13.5
25	0.3	100	2	0	40	12.1 ± 0.30	12.9 ± 0.59	8.7 ± 0.32	8.4
26	0.3	100	2	0	70	14.2 ± 0.30	17.8 ± 1.72	7.3 ± 0.72	10.5
27	0.3	100	2	0	100	21.2 ± 0.82	33.7 ± 2.10	7.5 ± 0.71	12.5

Source(s): Table by authors

algorithms could streamline the development of ANN architectures. Such advancements would alleviate dependence on researcher intuition, offering a more systematic and scalable pathway to enhance prediction accuracy and model robustness in complex systems.

This study addresses a key research gap by evaluating the performance of the fitrnet neural network regression model introduced in MATLAB 2022®. What sets this model apart is its ability to autonomously optimise a wide range of hyperparameters, including the number of hidden layers, neurons, activation functions and the regularisation parameter (lambda). To identify the optimal architecture, the exploration encompassed up to five hidden layers and 400 neurons. In addition, three widely used activation functions – relu, sigmoid and tanh – were systematically assessed to ensure a comprehensive evaluation of the model's capability. Because cross-validation was deployed, 90% of the data was used for training purpose and then the remaining 10% was used for testing and validation purposes. Recognising the extensive search domain, the limited-memory Broyden–Fletcher–Goldfarb–Shanno algorithm (LBFGS) and Bayesian optimisation approach were harnessed to streamline computational efficiency. Bayesian optimisation was chosen over grid search for its ability to efficiently explore high-dimensional hyperparameter spaces using fewer evaluations (Wu *et al.*, 2019). A mean squared error loss function is defined in equation (1):

$$MSE = \frac{1}{N}\sum_{i=1}^{N}\left(Y_i - \widehat{Y}_i\right)^2 \quad (1)$$

Throughout the training process, the Bayesian optimisation method orchestrated a reduction in cross-validation loss depicted as a function $m(x)$ in equation (2), where Y_i and $\widehat{Y}_i$ are the true and predicted values of the ith observation culminating in the determination of the optimal set of hyperparameters upon reaching the maximal objective evaluations. Notably, it was observed that the optimal architectural configuration did not invariably align with the final objective evaluation. Further insights into the hyperparameters optimisation process can be found in Table 3:

$$m(x) = \ln(1 + loss) = \ln(1 + MSE) \quad (2)$$

Figure 3 shows the ANN architecture used in current study with five inputs as layer thickness, printing speed, number of contours, raster angle and infill density and one single response as a separate model was built for TS, FS, IS and BT, respectively. For fastening the training process, all the inputs were normalised to [−1, 1] using equation (3), where X_n, X_r, $X_{r\min}$ *and* $X_{r\max}$ are the normalised, raw, minimum and maximum values of input parameters, respectively (Kumar *et al.*, 2022):

Table 3 Hyperparameters optimisation

Hyperparameters optimisation	
Type of network	Feedforward network
Optimisation method	Bayesian optimisation
Solver	Limited-memory Broyden–Fletcher–Goldfarb–Shanno algorithm (LBFGS)
Activations	Relu, Sigmoid, Tanh
Number of hidden layers range	[1, 5]
Number of hidden neurons range	[1 400]
Regularisation parameter lambda range	[2.4e-7, 2.4e + 3]
Maximum objective evaluations	60
K-fold cross-validation	10
Data division	Train set: 90%, Test set: 10%

Source(s): Table by authors

$$X_n = 2\frac{X_r - X_{r\min}}{X_{r\max} - X_{r\min}} - 1 \quad (3)$$

2.4 Optimisation

2.4.1 Multi-objective genetic algorithm

The optimisation of the five key FFF process parameters is crucial for ensuring optimal system performance. However, it should be acknowledged that achieving optimal conditions for one response variable may not necessarily coincide with optimal settings for others, potentially leading to conflicting objectives. This complexity underscores the need for multi-objective optimisation strategies, aiming to harmonise diverse and often conflicting goals. In this study, ANN models were integrated with a multi-objective GA to determine optimal conditions, concurrently optimising TS, FS, IS and BT. The goal was to maximise TS, FS and IS while minimising BT. In this work, multi-objective optimisation using GA was implemented in MATLAB 2022®. Maximum generations, population sizes and crossover fraction were 50, 200 and 0.8, respectively. GA originated from John Holland's work in the 1960s and draws inspiration from natural evolution by creating a population of potential solutions, selecting the best-performing individuals, applying genetic operations like crossover and mutation and iteratively evolving towards optimal solutions for complex optimisation problems (Katoch *et al.*, 2021). GA was used in this research due to its proven efficiency in identifying optimal process parameters with fewer iterations, as demonstrated by Esakki *et al.* (2021), where GA outperformed other methods in optimising selective inhibition sintering variables for IS.

2.4.2 TOPSIS method

In this study, TOPSIS was adopted to determine the best optimal parameters from sets of solutions provided by ANN-GA. TOPSIS plays a pivotal role in multi-objective optimisation by systematically ranking alternatives based on their closeness to both the ideal and anti-ideal solutions, aiding in informed decision-making. The primary steps of TOPSIS encompass the creation of a normalised decision matrix derived from the initial data, the calculation of a weighted normalised decision matrix with assigned weights for each criterion, the identification of ideal and anti-ideal solutions and subsequent computation of the distances of each alternative from these solutions. Ultimately, a preference index is derived through the comparison of distances, offering a ranked perspective on alternatives and guiding decision-making in those scenarios involving multiple criteria (Behzadian *et al.*, 2012; Dixit *et al.*, 2024). The entire TOPSIS process was implemented in MATLAB 2022®, using the data generated by the previous GA operation. The output is an Excel file containing the top ten solutions from the ANN-GA-TOPSIS workflows.

3. Results and discussion

3.1 Effect of key FFF process parameters on selected response

Table 5 presents the ANOVA results from Minitab® Statistical Software for the TS, and Figure 4 displays the main effect plots for the mechanical strength and BT. ANOVA was carried out to determine the significance of the five key FFF process parameters, reflected by the percentage of contribution and p-values < 0.05. The contribution of each factor was calculated as its sequential sum of squares divided by the total sequential

Figure 3 ANN model with five inputs and one output

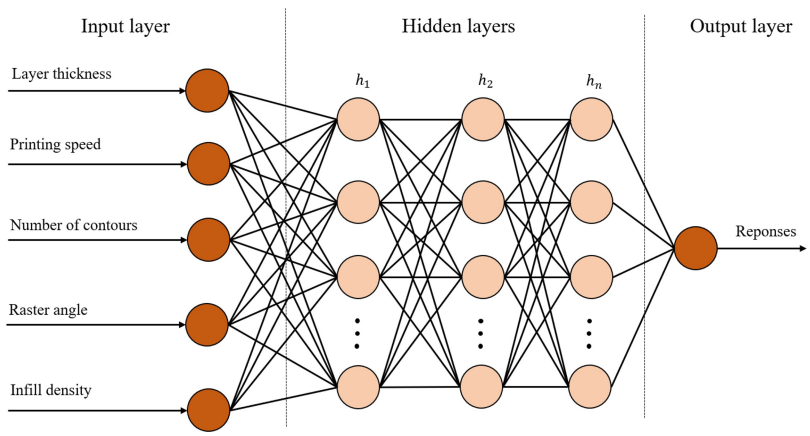

Source: Figure by authors

Figure 4 Main effects on tensile strength, flexural strength, impact strength and build time

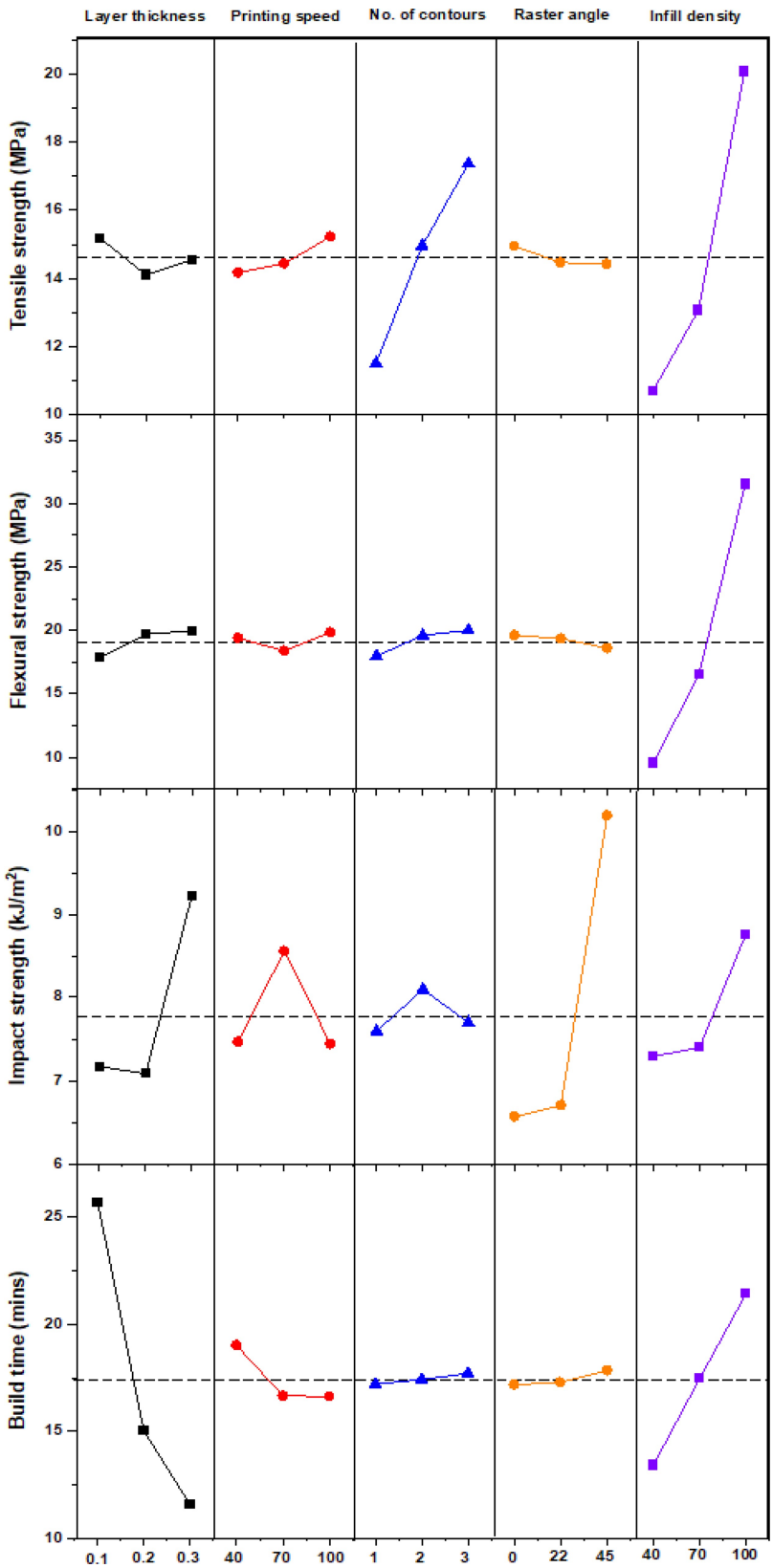

Source: Figure by authors

sum of squares, expressed as a percentage. The quadratic regression models were also fitted in Minitab® Statistical Software, and their *R*-squared values were recorded in Table 9. For TS, Table 4 reveals the infill density as the most significant factor with 60.6% of contribution, followed by the number of contours with 23.6% of contribution, agreed by Anand *et al.* (2025). It is interesting that the infill density does not affect in a linear fashion but in a quadratic pattern, illustrated by high *p*-value for the linear term ID but low *p*-value < 0.005 for the quadratic ID^2 term. This effect is also demonstrated in Figure 4 by an approximate parabolic curve when the infill density changes from 40% to 70%. In addition, the interaction term ID*NC, the two most influential factors, plays a significant role in the model with a low *p*-value. As shown in Figure 4, the change of infill density from 40% to 70% led to a rapid enhancement in TS. The improvement can be credited to the enhanced material bonding and reduced voids and defects inside the structure. This finding was confirmed by Tura *et al.* (2023) when setting 100% infill density resulted in the maximum TS of printed parts. A consistent upward trend in TS when the infill density changed from 20% to 100% obtained in Alafaghani and Qattawi (2018) further asserted the importance of infill density. Anand *et al.* (2025) concluded infill density to be the most influential factor and 100% infill would optimise the TS of 3D-printed PETG parts. As the contour consists of deposited filament aligned with the applied load, an increasing number of contours can lead to the enhancement in TS which is evident in (Giri *et al.*, 2021). Singh *et al.* (2019) investigated the impact of various process parameters on the TS of FFF-printed ABS/HIPS and concluded the optimal number of the contours to be three, the high value.

As illustrated in Figure 4, a discernible pattern emerges wherein the low value of layer thickness correlates with the maximum TS. This observation aligns with existing research, as the reduction in layer thickness facilitates finer inter-layer bonding, thereby mitigating the likelihood of delamination and surface defects (Wang *et al.*, 2020; Dev and Srivastava, 2023; Singh *et al.*, 2019; Pazhamannil *et al.*, 2021). The TS was found to reach the lowest point at 0.2 mm and increase again at 0.3 mm. According to Singh *et al.* (2019), altering the raster angle led to variations in TS along different axes and with typical anisotropy behaviours of FFF-printed materials (Zohdi and Yang, 2021), the TS is direction-dependent. While the maximum TS was often found at 0° (Fountas *et al.*, 2022; Bakır *et al.*, 2021; Dev and Srivastava, 2023), the current work observed the maximum TS attained at 45° raster angle though the main effect plots in Figure 4 still show a slight downward trend when the raster angle increases. Indeed, this finding is supported by the low significance of the raster angle, evidenced in Figure 4, and the reduced sensitivity of HIPS to the anisotropy effect (Zohdi and Yang, 2019). In a recent study, after analysing ANOVA and main effect plots results, low printing speed was recommended to attain high TS (Chinchanikar *et al.*, 2024). However, in this work, printing at high speed is proved to attain good TS. This could be due to the essence of the FFF-printed feedstocks or printer performance.

For the FS, infill density remains the predominant contributor with 89.8%, based on Table 5 while other factors demonstrate insignificant contributions, agreed by (Chinchanikar *et al.*, 2024). Similar to the TS, based on the *p*-value, the linear term ID does not show any significances while the quadratic term ID^2 appears to be the most influential. Similar parabolic pattern is illustrated in Figure 4 when the infill density increases from 40% to 70%. In addition, the interaction term NC*ID proves the combined impact of number of contours and infill density on the FS. Higher infill density results in a denser structure, thereby enhancing FS, a conclusion supported by Atakok *et al.* (2022) and Dev and Srivastava (2023). In Singh *et al.*'s (2019) study, when the infill density was varied at three levels (20%, 50% and 80%), a different trend was reported as the maximum was recorded at the medium level. The main reason was attributed to the delamination occurred when above 50% infill density is applied. However, the specimens in the current study did not experience the same issue.

As the contours behave as peripheral shields and help the parts sustain the applied load (Singh *et al.*, 2019), increasing the number of contours enhanced the FS of the specimens, as

Table 4 ANOVA results for tensile strength

Source	DF	Seq SS	Contribution (%)	Adj SS	Adj MS	*f*-value	*p*-value
Regression	14	638.726	97.22	638.726	45.6233	30.02	0.000
LT	1	1.767	0.27	0.748	0.7483	0.49	0.496
PS	1	4.895	0.75	1.182	1.1825	0.78	0.395
NC	1	155.118	23.61	22.820	22.8195	15.02	0.002
RA	1	1.271	0.19	1.233	1.2330	0.81	0.385
ID	1	398.128	60.60	2.238	2.2383	1.47	0.248
LT*LT	1	3.491	0.53	3.491	3.4915	2.30	0.155
PS*PS	1	0.399	0.06	0.399	0.3994	0.26	0.617
NC*NC	1	1.673	0.25	1.673	1.6732	1.10	0.315
RA*RA	1	0.329	0.05	0.329	0.3295	0.22	0.650
ID*ID	1	32.216	4.90	32.216	32.2156	21.20	0.001
LT*ID	1	7.326	1.12	7.326	7.3258	4.82	0.049
PS*ID	1	5.158	0.79	5.158	5.1581	3.39	0.090
NC*ID	1	26.466	4.03	26.466	26.4657	17.42	0.001
RA*ID	1	0.488	0.07	0.488	0.4883	0.32	0.581
Error	12	18.234	2.78	18.234	1.5195		
Total	26	656.960	100.00				

Source(s): Table by authors

Table 5 ANOVA results for flexural strength

Source	DF	Seq SS	Contribution (%)	Adj SS	Adj MS	*F*-value	*p*-value
Regression	14	2387.72	98.89	2387.72	170.552	76.62	0.000
LT	1	19.18	0.79	5.76	5.760	2.59	0.134
PS	1	0.94	0.04	2.64	2.637	1.18	0.298
NC	1	18.19	0.75	22.35	22.349	10.04	0.008
RA	1	4.49	0.19	0.14	0.143	0.06	0.804
ID	1	2167.00	89.75	0.15	0.150	0.07	0.799
LT*LT	1	3.43	0.14	3.43	3.435	1.54	0.238
PS*PS	1	9.24	0.38	9.24	9.244	4.15	0.064
NC*NC	1	2.26	0.09	2.26	2.260	1.02	0.334
RA*RA	1	0.33	0.01	0.33	0.334	0.15	0.705
ID*ID	1	96.53	4.00	96.53	96.533	43.37	0.000
LT*ID	1	0.11	0.00	0.11	0.105	0.05	0.832
PS*ID	1	11.26	0.47	11.26	11.265	5.06	0.044
NC*ID	1	54.33	2.25	54.33	54.326	24.41	0.000
RA*ID	1	0.42	0.02	0.42	0.420	0.19	0.672
Error	12	26.71	1.11	26.71	2.226		
Total	26	2414.43	100.00				

Source(s): Table by authors

depicted in Figure 4 and agreed in Gebisa and Lemu (2018) and Singh *et al.* (2019). The results also show that the contours appear to have a lower impact on FS than TS. Furthermore, FS exhibited a rapid increase from low to medium layer thickness levels, with a subsequent marginal rise at high layer thickness levels, a trend affirmed by Atakok *et al.* (2022) in their study on 3D-printed PLA. Many studies highlighted raster angle (Gebisa and Lemu, 2018; Fountas *et al.*, 2022) as a significant factor in FS but in correlation with infill density, the raster angle does not exhibit any profound effects. Interestingly, current results suggest printing at high speed for optimum FS while Chahdoura *et al.* (2025) and Chinchanikar *et al.* (2024) advocated low printing speed for 3D-printed PLA and ABS parts. This highlights the unique properties of HIPS, which enable faster printing while preserving mechanical integrity, ultimately reducing BT. For the IS, raster angle plays a critical role with 41.2% of contribution, followed by layer thickness with 13.0% of contribution. The ANOVA results in Table 6 confirmed the significance of RA^2, PS^2, PS*ID, LT, RA and PS with *p*-values less than 0.05. Although the increase in infill density still leads to higher IS, the effect of infill density is not comparable with those from raster angle and layer thickness. Ramesh and Panneerselvam (2021) and Singh *et al.* (2019) also discovered a similar trend for infill density in enhancing IS. This finding appeared to shed a light on the contribution of raster angle because without considering this factor, infill density was affirmed to be the most influential for the 3D-printed ABS parts (Chinchanikar *et al.*, 2024). Another study also indicated the importance of raster angle on the 3D-printed performance (Anerao *et al.*, 2024). As opposed to the findings for TS and FS, the maximum IS was attained at two contours and exceeding this value causes impairment to the property. While printing at a high speed was proposed for optimising TS and FS, medium speed is recommended for IS. While Kamaal *et al.* (2021) recommended a low level of layer thickness for optimum IS for PLA/carbon-fibre, the current research reveals a high level of layer thickness for maximising IS, as depicted in Figure 4.

Layer thickness predominantly affects the BT with 65.9% of contribution and infill density maintains its second place with 21.1% of contribution. In Table 7, with *p*-values less than 0.05, the significant terms are LT^2, PS^2, LT*ID, LT, PS and ID. Transitioning layer thickness from 0.1 to 0.3 mm results in a notable reduction in BT while more time is required to fabricate parts at a higher infill density. Kumar *et al.* (2022) similarly identified the noteworthy influence of layer thickness while pursuing optimisation of BT and SR. In a separate investigation, layer thickness emerged as the most influential factor with a contribution of 84.6%, highlighting its significance in achieving reduced BT, particularly at lower layer thickness levels (Wankhede *et al.*, 2020). It was also confirmed after optimisation, high layer thickness would lead to a reduction of at least 5% in BT (Dixit *et al.*, 2024). Intuitively, elevating the printing speed should logically reduce the printing duration, as agreed by Kumar *et al.* (2022). When the BT considers the geometrical impact of all testing samples, adjusting the printing speed from 40 to 70 mm/s results in a significant reduction in the BT with the minimum BT suggested at 100 mm/s. Notably, while the number of contours plays a pivotal role in enhancing mechanical strength, its influence on BT remains relatively insignificant. Hence, when the printing geometry and conditions permit a substantial number of contours, printing the parts with a reasonable number of contours can boost the strength without compromising on the BT.

Table 6 ANOVA results for impact strength

Source	DF	Seq SS	Contribution (%)	Adj SS	Adj MS	*F*-value	*p*-value
Regression	14	136.396	93.70	136.396	9.7426	12.74	0.000
LT	1	18.900	12.98	2.441	2.4411	3.19	0.099
PS	1	0.005	0.00	11.585	11.5845	15.15	0.002
NC	1	0.057	0.04	2.248	2.2481	2.94	0.112
RA	1	59.910	41.15	6.213	6.2129	8.13	0.015
ID	1	9.665	6.64	0.068	0.0682	0.09	0.770
LT*LT	1	7.432	5.11	7.432	7.4315	9.72	0.009
PS*PS	1	7.266	4.99	7.266	7.2664	9.50	0.009
NC*NC	1	0.943	0.65	0.943	0.9434	1.23	0.288
RA*RA	1	16.125	11.08	16.125	16.1247	21.09	0.001
ID*ID	1	2.265	1.56	2.265	2.2646	2.96	0.111
LT*ID	1	0.910	0.63	0.910	0.9101	1.19	0.297
PS*ID	1	7.186	4.94	7.186	7.1863	9.40	0.010
NC*ID	1	2.338	1.61	2.338	2.3381	3.06	0.106
RA*ID	1	3.395	2.33	3.395	3.3945	4.44	0.057
Error	12	9.175	6.30	9.175	0.7646		
Total	26	145.571	100.00				

Source(s): Table by authors

Table 7 ANOVA results for build time

Source	DF	Seq SS	Contribution (%)	Adj SS	Adj MS	*F*-value	*p*-value
Regression	14	1358.88	99.61	1358.88	97.0631	218.83	0.000
LT	1	898.88	65.89	87.93	87.9307	198.24	0.000
PS	1	26.08	1.91	7.88	7.8789	17.76	0.001
NC	1	1.01	0.07	0.32	0.3160	0.71	0.415
RA	1	2.02	0.15	0.00	0.0045	0.01	0.921
ID	1	287.47	21.07	21.12	21.1200	47.61	0.000
LT*LT	1	79.05	5.79	79.05	79.0453	178.20	0.000
PS*PS	1	7.96	0.58	7.96	7.9606	17.95	0.001
NC*NC	1	0.02	0.00	0.02	0.0161	0.04	0.852
RA*RA	1	0.24	0.02	0.24	0.2400	0.54	0.476
ID*ID	1	0.01	0.00	0.01	0.0139	0.03	0.862
LT*ID	1	52.36	3.84	52.36	52.3615	118.05	0.000
PS*ID	1	1.66	0.12	1.66	1.6626	3.75	0.077
NC*ID	1	2.08	0.15	2.08	2.0833	4.70	0.051
RA*ID	1	0.04	0.00	0.04	0.0431	0.10	0.761
Error	12	5.32	0.39	5.32	0.4436		
Total	26	1364.21	100.00				

Source(s): Table by authors

3.2 Artificial neural network models

Upon conducting 60 evaluations, the architectural optimisation for ANN models concluded, encompassing all hyperparameters, are outlined in Table 8. Interestingly, the predictive model for BT necessitates only one layer and 288 neurons, whereas the others necessitate a minimum of four layers. Evidently, executing this process using a standard manual approach proves impractical due to the requirement for up to 378 maximum hidden neurons. Figure 5 shows the regression plots of TS [Figure 5(a)], FS [Figure 5(b)], IS [Figure 5(c)] and BT of FFF-printed HIPS [Figure 5(d)]. As observed in Figure 5, the optimisation process was notably successful, as evidenced by the correlation coefficient *R* of the ANN models predicting TS, FS, IS and BT, respectively. The *R*-squared values of the ANN models were calculated and compared with the Regression models in Table 9. ANN models demonstrated better fitting accuracies for all

Table 8 Optimal ANN architecture

Response	No. of hidden layers	Activations	Lambda	No. of neurons in each hidden layer				
				Layer 1	Layer 2	Layer 3	Layer 4	Layer 5
Tensile strength	3	Relu	5.14e-6	378	321	47	57	35
Flexural strength	4	Relu	1.59	30	93	119	3	352
Impact strength	1	Relu	0.20	58	61	198	10	–
Build time	4	Relu	4.55e-3	288	–	–	–	–

Source(s): Table by authors

Figure 5 Regression plots corresponding to optimal training algorithm for (a) tensile strength; (b) flexural strength; (c) impact strength; and (d) build time

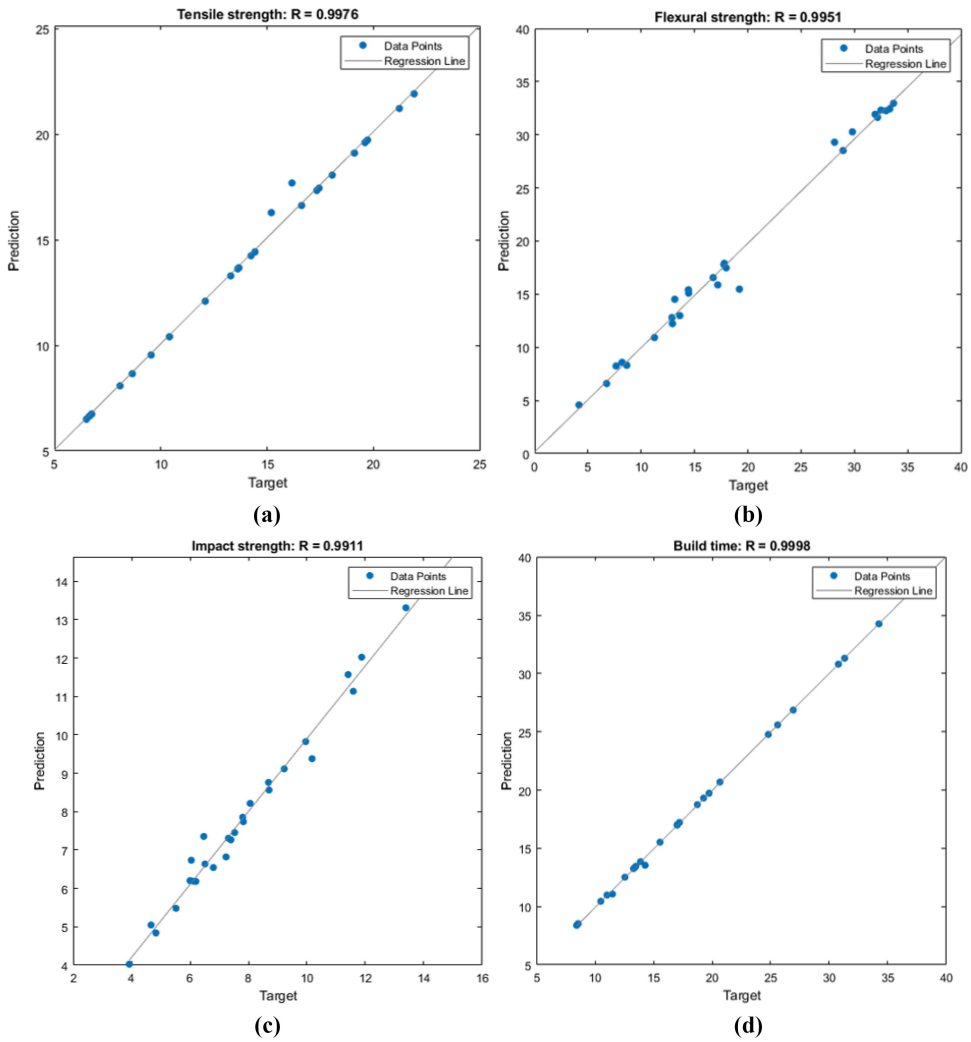

Source: Figure by authors

properties compared to the Regression models. After developing the Regression models, Alafaghani *et al.* (2021) had the same findings and concluded the second-order models were not sufficient to capture the non-linear effect of process parameters on the properties of FFF-printed parts.

The obtained results reveal the limitations of using a restricted ANN design with only up to three hidden layers and a low neuron count, which proved insufficient for accurately capturing surface roughness patterns under varying process parameters like layer thickness, infill density, printing speed and extrusion temperature, leading to poor predictive accuracy (Chinchanikar *et al.*, 2022). To overcome the shortcomings of trial-and-error methods in ANN initialisation, Meiabadi *et al.* (2021) introduced a GA to optimise ANN performance, enhancing its adaptability to complex data sets. Similarly, another study addressed the pitfalls of manual calibration by aggregating outputs from 36 separate networks, achieving improved accuracy compared to a single network approach

Table 9 R^2 values of response parameters using regression and ANN models

Response parameter	R^2(Regression)	R^2(ANN)
Tensile strength	0.9722	0.9952
Flexural strength	0.9889	0.9902
Impact strength	0.9370	0.9823
Build time	0.9961	0.9996

Source(s): Table by authors

(Alafaghani *et al.*, 2021). Despite their advancements, these methods are intricate and resource intensive. In contrast, the approach proposed in this study offers a more streamlined alternative by automating architecture optimisation, significantly reducing complexity and making it accessible even to researchers without extensive expertise in ANN design.

4. Optimisation and validation

4.1 Optimisation of mechanical properties and build time of FFF-printed HIPS

The chosen objectives inherently oppose one another, requiring the maximisation of TS, FS and IS while concurrently minimising BT. To address this dilemma, a multi-objective GA in MATLAB 2022® was applied to optimise ANN models, effectively identifying a comprehensive range of optimised parameter sets. The constraints are $0.1 \leq LT \leq 0.3$, $40 \leq PS \leq 100$, $1 \leq NC \leq 3$, $0 \leq RA \leq 45$ and $40 \leq ID \leq 100$. To address the multi-objective nature of the problem, specialised techniques were used to compare and rank individuals based on their performance across different objectives. These techniques help identify a set of solutions known as Pareto optimal solutions. The Pareto front represents the trade-offs between the objectives, where improving one objective may lead to a degradation in another. Because the main objective was to strike the balance between properties, the weight for each property was 0.25. After acquiring the list of optimal solutions ranked by TOPSIS, it was observed that the numerical values of top solutions were closely clustered and not practically achievable for the 3D printer. Consequently, for each solution, the numerical values of raster angle and number of contours were approximated to the nearest integer; the printing speed and infill density were rounded to the nearest ten; and the layer thickness values were rounded to the nearest two decimal points. For example, if the original TOPSIS solutions resulted in 0.202 mm LT, 88 mm/s PS, 2.2 NC, 42.3° RA and 92% ID, the adjusted solutions would be 0.20 mm LT, 90 mm/s PS, 2 NC, 42° RA and 90% ID. Subsequently, an additional step was executed to eradicate identical solutions before feeding the inputs into ANN models for generating new predictive TS, FS, IS and BT. In the end, TOPSIS was carried out again to rank the solutions using appropriate weights for the four responses. With this procedure, the adjusted TOPSIS tables covered a wider range of possible solutions for optimisation.

Table 10 lists the set of optimal solutions for every ANN model, where "Sol No." indicates the solution number. The ANN-GA-TOPSIS method resulted in 18.2 MPa TS, 33.7 MPa FS and 14.1 MPa IS and 14.1 min BT corresponding to 0.29 mm LT, 50 mm/s PS, 1 NC, 44° RA and 100% ID. In an overview, the proposed methodologies led to predicted enhancement in response parameters.

Table 11 presents various sets of process parameters with different optimisation properties. The notations "MaxTS", "MaxFS", "MaxIS" and "MinBT" are used to represent the set of five key FFF process parameters that achieved the maximum TS, FS, IS and the minimum BT, respectively. Meanwhile, the notation "ANN-GA-TOPSIS" is used for the set of those process parameters that aim to optimise and harmonise all the selected responses. The errors between experimental and predicted values of ANN-GA-TOPSIS are only 6.6%, 2.9%, 6.6% and 2.9% for TS, FS, IS and BT, respectively, asserting the potency of this model in predicting mechanical strength and BT.

4.2 Sensitivity analysis on mechanical properties and build time of FFF-printed HIPS

Sensitive analysis was conducted to evaluate the robustness of the optimal solution by revealing how small variation (±5%) in process parameters can influence the predicted performance (Ali and Esakki, 2020). Figure 6 illustrates the results of sensitive analysis on TS [Figure 6(a)], FS [Figure 6(b)], IS [Figure 6(c)] and BT of FFF-printed HIPS [Figure 6(d)]. It is worth noting that if the high and low values exceeded the upper and lower bounds, the bounded values were used as inputs to the predictive models, for example, for RA and ID. Because the NC is a discrete variable (e.g., 1, 2, 3), the ±5% variation was rounded to the nearest valid integers, resulting in 1 and 2 being considered as the low and high values, respectively. In general, small changes in the inputs did not generate high impacts on the outputs. According to Figure 6(a) and (b), it is confirmed

Table 10 A family of optimal solutions obtained by GA-ANN-TOPSIS

Sol no.	LT	PS	NC	RA	ID	Tensile strength (MPa)	Flexural strength (MPa)	Impact strength (kJ/m^2)	Build time (min)	Ranking
1	0.29	50	1	44	100	18.2	33.7	14.1	14.4	1
2	0.29	60	1	38	100	18.3	33.4	12.5	13.8	2
3	0.26	50	1	44	100	18.3	33.6	13.3	15.7	3
4	0.11	40	1	44	100	22.6	33.3	12.5	35.7	4
5	0.25	50	1	44	100	18.4	33.5	13.0	16.3	5
6	0.13	60	1	44	100	22.8	32.4	10.9	30.3	6
7	0.17	50	1	44	100	20.5	33.1	11.8	24.4	7
8	0.10	40	2	44	100	21.9	32.2	12.3	35.3	8
9	0.11	40	2	44	100	21.4	32.2	12.1	33.6	9
10	0.11	60	2	44	100	22.6	30.4	10.6	32.0	10

Source(s): Table by authors

Table 11 Process parameters and their responses

Particular	Parameter	MaxTS	MaxFS	MaxIS	MinBT	ANN-GA-TOPSIS
Optimised parameters	LT (mm)	0.1	0.3	0.3	0.3	0.29
	PS (mm/s)	100	100	70	100	50
	NC	3	**2**	1	2	1
	RA (°)	45	0	45	0	44
	ID (%)	100	100	100	40	100
Experiment responses	TS (MPa)	24.0 ± 1.04	21.2 ± 0.82	18.0 ± 0.84	12.1 ± 0.30	17.1 ± 1.02
	FS (MPa)	28.9 ± 1.95	33.7 ± 2.10	32.2 ± 1.32	12.9 ± 0.59	32.8 ± 1.77
	IS (kJ/m^2)	10.0 ± 0.69	7.5 ± 0.71	13.4 ± 0.88	8.7 ± 0.32	13.2 ± 0.47
	BT (min)	31.3	12.5	13.5	8.4	14.0

Source(s): Table by authors

Figure 6 Sensitive analysis on (a) tensile strength, (b) flexural strength, (c) impact strength and (d) build time of FFF-printed HIPS

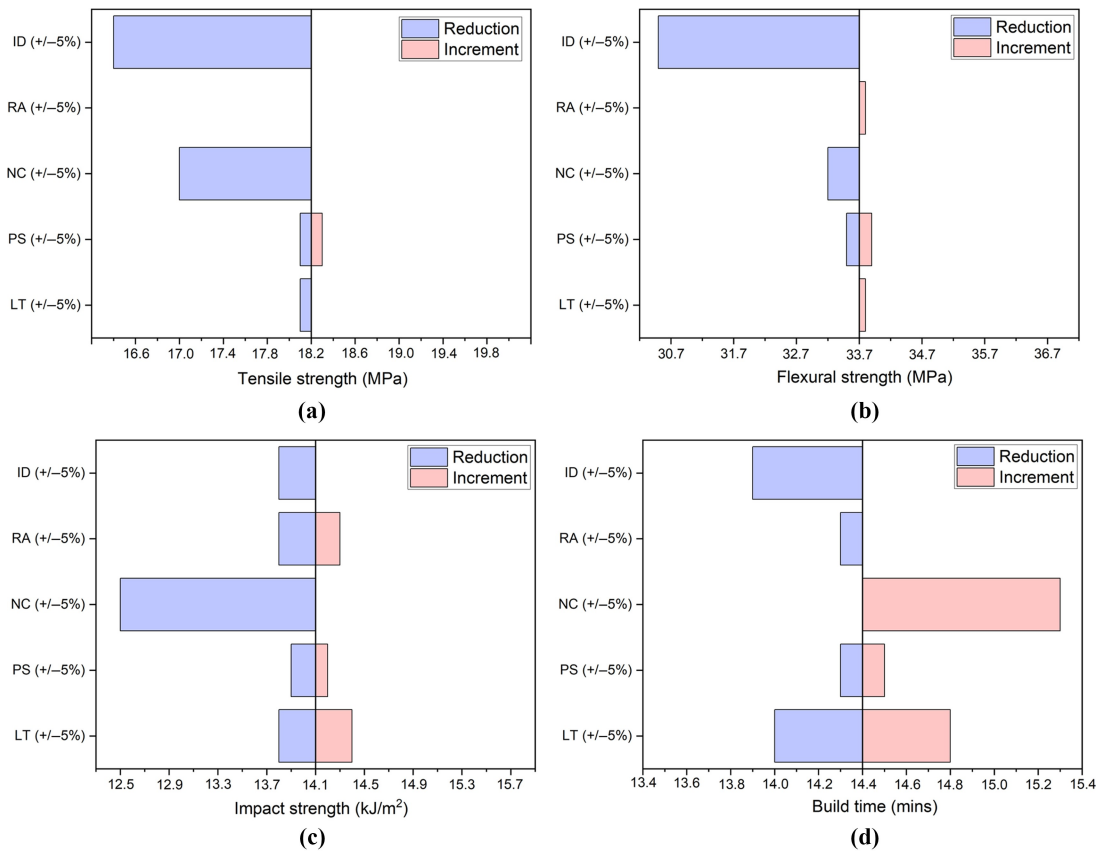

Source: Figure by authors

that a 5% reduction in ID contributed to a decrease of 8.8% and 8.9% of TS and FS, respectively. Meanwhile, from Figure 6(c) and (d), 5% variations of NC led to an 11.5% reduction in IS and a 6.3% increase in BT. Overall, these small variations do not cause significant changes in performance and remained within the acceptable range, thereby validating the robustness of the optimal parameters determined.

4.3 Comparison of mechanical properties and build time of FFF-printed HIPS

Figure 7 compares the selected properties of different optimum sets presented in Table 11. For this material, achieving the optimum TS for MaxTS leads to a tremendous BT, approximately 2.2 times greater than that of ANN-GA-TOPSIS. In contrast, attaining the minimum BT for MinBT reduces the TS, FS and IS by 29%, 61% and 34%, respectively, when compared to ANN-GA-TOPSIS.

From the properties of ANN-GA-TOPSIS shown in Figure 7, it is concluded that maximising all mechanical strength and minimising the BT is unattainable for this material. Alafaghani *et al.* (2021) reached the same conclusions when attempting to maximise the strength and minimise dimensional error. Specifically, the FS and IS of ANN-GA-TOPSIS are only 2.7% and 1.5% lower than the optimum FS

Figure 7 Comparisons of selected properties of HIPS 3D-printed specimens at various sets of five key FFF process parameters

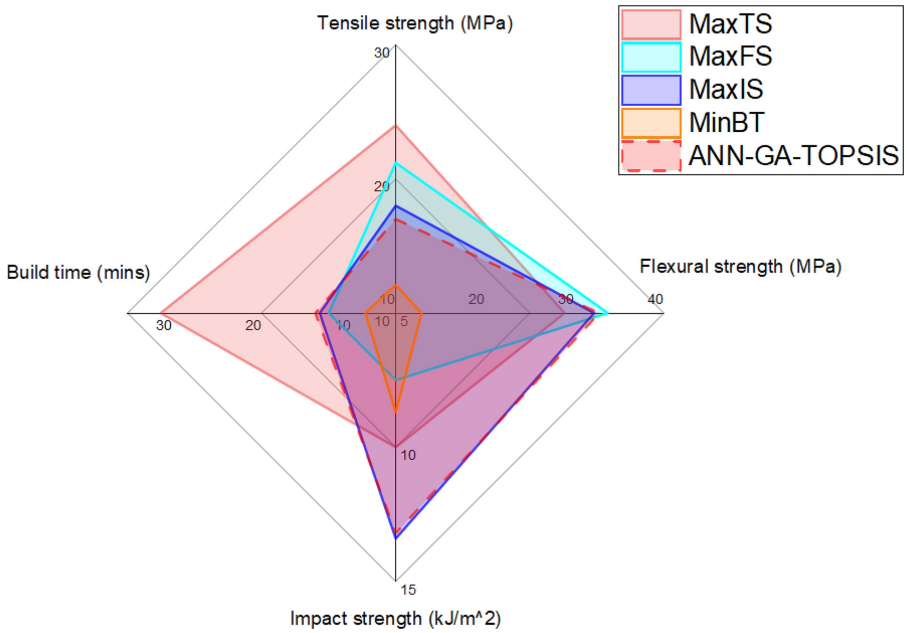

Source: Figure by authors

and IS offered by MaxFS and MaxIS. Meanwhile, the TS of ANN-GA-TOPSIS suffered a huge reduction of 28.9% compared to MaxTS. In addition, though the BT for ANN-GA-TOPSIS cannot reach the minimum, a significant reduction of 55% compared to MaxTS is attained. Hence, ANN-GA-TOPSIS is concluded to achieve a reasonable balance and harmony for FS, IS and BT while the TS is compromised. That is the reason why Singh *et al.* (2019) suggested mixing HIPS with ABS for creating automotive parts with high IS while maintaining elasticity.

The outcomes of this research can be leveraged in medical field where HIPS-based 3D-printed components such as prosthetic foot and knee (Algarín Roncallo *et al.*, 2024) or implants (Balasubramainian *et al.*, 2024) can be used. And the optimal set of process parameters can guarantee a balance between mechanical strength and BT which are critical for cost-effective and high-quality production. In addition, the application can be expanded to electronics, for example, FFF-printed HIPS beam-shaping components for terahertz range (Stanaitis *et al.*, 2024). The optimised material can be deployed further to design practical components based on the concept of design for AM (Chahdoura *et al.*, 2025; Asadollahi-Yazdi *et al.*, 2019). Beyond HIPS, our framework can be adapted to optimise various materials and printing systems, offering a scalable solution for industries seeking to enhance mechanical properties while minimising manufacturing time, thereby advancing the capabilities of AM across multiple domains.

5. SEM and fractography

Figure 8 compares the SEM images captured at ×25 between the tensile specimens of MaxTS [Figure 8(a)] and ANN-GA-TOPSIS [Figure 8(d)], between the flexural specimens of MaxFS [Figure 8(b)] and ANN-GA-TOPSIS [Figure 8(e)] and between the impact specimens of MaxIS [Figure 8(c)] and ANN-GA-TOPSIS [Figure 8(f)]. The main goal is to identity the differences in fractography which affects the printed properties.

Tensile specimen of MaxTS in Figure 8(a) demonstrated a denser structure with less air voids between deposited filaments and layers than its counterpart in Figure 8(d). It was due to the low layer thickness of 0.1 mm as compared to 0.3 mm of the ANN-GA-TOPSIS, explaining the reduction of 28.9% in TS. A dense structure similar to Figure 8(a) was confirmed to achieve better mechanical performance in literature (Wang *et al.*, 2020; Deshwal *et al.*, 2020). Comparing the flexural specimens in Figures 8(b) and (e), reveals minimal structural differences, which aligns with the similar properties observed in Section 4. In addition, the original circular filament was deformed into a trapezoidal shape, consistent with findings reported in the literature for 3D-printed ABS structures (Vidakis *et al.*, 2021; Abeykoon *et al.*, 2020). Like the flexural specimens, the impact specimens shown in Figure 8(c) and (f), exhibit minimal structural differences, which accounts for the small variation of 1.5% in their properties.

6. Conclusions

This research develops a material optimisation framework with mixing experimental and theoretical analysis procedures for FFF of thermoplastic polymers. Through the multi-criteria decision-making process and ANN-GA-TOPSIS optimisation model, the five key FFF process parameters can be optimised to enhance the material properties of FFF-printed thermoplastic materials for wider applications in practice. The devised multi-objective model was validated using the obtained experimental data.

The discussion on research findings and results yields subsequent conclusions as follows:

Figure 8 SEM images of specimens: (a) Tensile for MaxTS; (b) flexural for MaxFS; (c) Charpy for MaxIS; (d) tensile for ANN-GA-TOPSIS; (e) flexural for ANN-GA-TOPSIS; and (f) Charpy for ANN-GA-TOPSIS

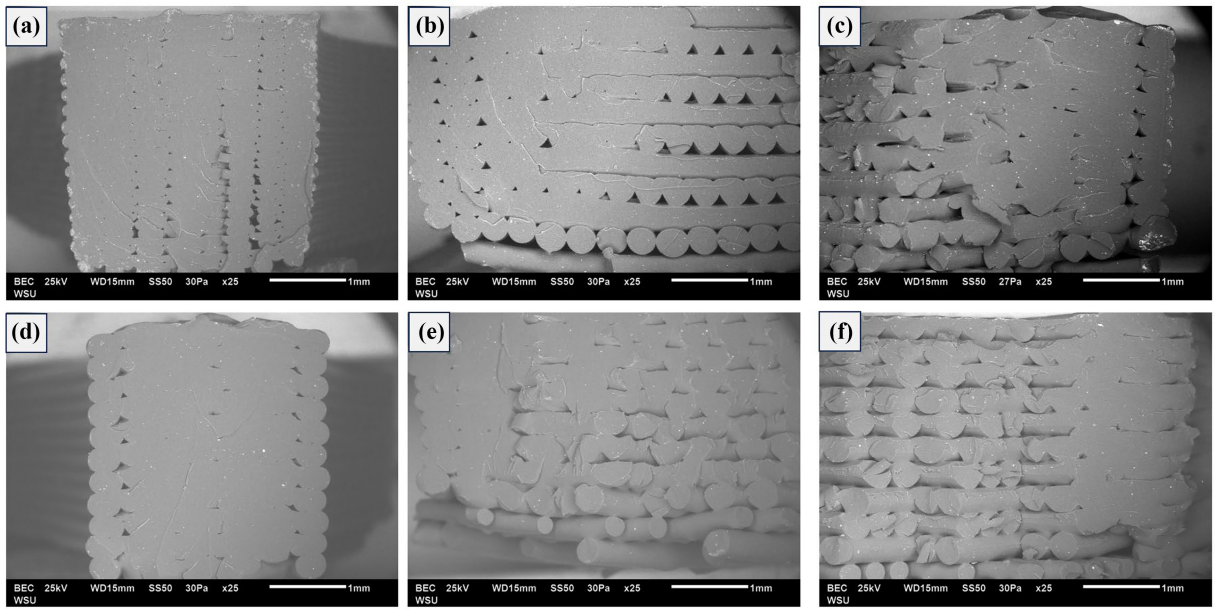

Source: Figure by authors

- For TS, the maximum value was attained at Run 9 with 0.1 mm LT, 100 mm/s PS, 3 NC, 45°C RA and 100% ID and infill density was found to be the most significant factor.
- For FS, the optimum value was attained at Run 27 with 0.3 mm LT, 100 mm/s PS, 2 NC, 0°C RA and 100% ID and infill density was found to be the most significant factor.
- For IS, the maximum value was attained at Run 24 with 0.3 mm LT, 70 mm/s PS, 1 NC, 45°C RA and 100% ID and raster angle was found to be the most significant factor.
- For BT, the optimum value was attained at Run 25 with 0.3 mm LT, 100 mm/s PS, 2 NC, 0°C RA and 40% ID and layer thickness was found to be the most significant factor.
- After performing multi-objective optimisation, ANN-GA-TOPSIS was found to compromise 28.9%, 2.7% and 1.5% of TS, FS, IS to reduce the BT by 55%, corresponding to 0.29 mm LT, 50 mm/s PS, 1 NC, 44°C RA and 100% ID. The optimum set can be used to print high-performance parts for automotive industries and medical fields with rational fabrication time.

Although the multi-objective optimisation revealed the most harmonised and attainable performance for HIPS, maximising mechanical strength and minimising BT simultaneously was not feasible. However, the findings of this study hold significant implications for designers and manufacturers of domestic and small industrial components, aiding in the comprehensive understanding of how process parameters collectively influence part characteristics. Future research can adopt this optimisation framework to perform multi-objective optimisation for other part qualities such as surface roughness and dimensional accuracy. The number of varied process parameters can be expanded to provide a more comprehensive understanding on the effect of process parameters on the 3D-printed parts. Furthermore, the approach proposed in this study bears relevance for various applications, whether involving diverse materials or response parameters.

Acknowledgements

The first author sincerely shows gratitude to Graduate Research School, Western Sydney University, for financial support on his PhD study via the Postgraduate Scholarship Awards. Technical supports from the Teaching Research Technical Services (TRTS) and the Advanced Materials Characterisation Facility (AMCF) at Western Sydney University are acknowledged by all authors.

References

Abeykoon, C., Sri-Amphorn, P. and Fernando, A. (2020), "Optimization of fused deposition modeling parameters for improved PLA and ABS 3D printed structures", *International Journal of Lightweight Materials and Manufacture*, Vol. 3 No. 3, pp. 284-297.

Alafaghani, A. and Qattawi, A. (2018), "Investigating the effect of fused deposition modeling processing parameters using Taguchi design of experiment method", *Journal of Manufacturing Processes*, Vol. 36, pp. 164-174.

Alafaghani, A., Ablat, M.A., Abedi, H. and Qattawi, A. (2021), "Modeling the influence of fused filament fabrication processing parameters on the mechanical properties of ABS parts", *Journal of Manufacturing Processes*, Vol. 71, pp. 711-723.

Alarifi, I.M. (2023), "PETG/carbon fiber composites with different structures produced by 3D printing", *Polymer Testing*, Vol. 120, p. 107949.

Algarín Roncallo, R.J., Lopez Taborda, L.L. and Guillen, D. (2024), "Experimental characterization, theoretical modeling and failure analysis of the mechanical behavior of acrylonitrile butadiene styrene parts by fused filament fabrication", *Rapid Prototyping Journal*, Vol. 30 No. 1, pp. 145-160.

Ali, T.K. and Esakki, B. (2020), "Study on compressive strength characteristics of selective inhibition sintered UHMWPE specimens based on ANN and RSM approach", *CIRP Journal of Manufacturing Science and Technology*, Vol. 31, pp. 281-293.

Almutairi, M.D., Mascarenhas, T.A., Alnahdi, S.S., He, F. and Khan, M.A. (2023), "Modal response of hybrid raster orientation on material extrusion printed acrylonitrile butadiene styrene and polyethylene terephthalate glycol under thermo-mechanical loads", *Polymer Testing*, Vol. 120, p. 107953.

Anand, S., Dhankhar, G. and Satyarthi, M.K. (2025), "Optimizing mechanical properties of PETG fabricated parts via PSO-BFO hybrid algorithm in fused deposition modelling", *International Journal on Interactive Design and Manufacturing (IJIDeM)*, Vol. 19 No. 8.

Anerao, P., Kulkarni, A. and Munde, Y. (2024), "A review on exploration of the mechanical characteristics of 3D-printed biocomposites fabricated by fused deposition modelling (FDM)", *Rapid Prototyping Journal*, Vol. 30 No. 3, pp. 430-440.

Asadollahi-Yazdi, E., Gardan, J. and Lafon, P. (2019), "Multi-objective optimization approach in design for additive manufacturing for fused deposition modeling", *Rapid Prototyping Journal*, Vol. 25 No. 5, pp. 875-887.

Atakok, G., Kam, M. and Koc, H.B. (2022), "Tensile, three-point bending and impact strength of 3D printed parts using PLA and recycled PLA filaments: a statistical investigation", *Journal of Materials Research and Technology*, Vol. 18, pp. 1542-1554.

Bakır, A.A., Atik, R. and Özerinç, S. (2021), "Effect of fused deposition modeling process parameters on the mechanical properties of recycled polyethylene terephthalate parts", *Journal of Applied Polymer Science*, Vol. 138 No. 3, p. 49709.

Balasubramainian, N.K., Kothandaraman, L., Sathish, T., Giri, J. and Ammarullah, M.I. (2024), "Optimization of process parameters to minimize circularity error and surface roughness in fused deposition modelling (FDM) using Taguchi method for biomedical implant fabrication", *Advanced Manufacturing: Polymer & Composites Science*, Vol. 10 No. 1.

Behzadian, M., Otaghsara, S.K., Yazdani, M. and Ignatius, J. (2012), "A state-of the-art survey of TOPSIS applications", *Expert Systems with Applications*, Vol. 39 No. 17, pp. 13051-13069.

Ben Rezg, M., Nasser, M., Othmani, R. and Montagne, A. (2025), "Multi-criteria selectivity of PLA polymer 3D printing parameters: impact on the roughness of finished surfaces", *Progress in Additive Manufacturing*, Vol. 10 No. 9.

Bregoli, C., Fiocchi, J., Biffi, C.A. and Tuissi, A. (2024), "Additively manufactured medical bone screws: an initial study to investigate the impact of lattice-based Voronoi structure on implant primary stability", *Rapid Prototyping Journal*, Vol. 30 No. 1, pp. 60-72.

Cerro, A., Romero, P.E., Yigit, O. and Bustillo, A. (2021), "Use of machine learning algorithms for surface roughness prediction of printed parts in polyvinyl Butyral via fused deposition modeling", *The International Journal of Advanced Manufacturing Technology*, Vol. 115 Nos 7-8, pp. 2465-2475.

Chahdoura, S., Bahloul, R., Tlija, M. and Tahan, A. (2025), "Multi-objective optimization of PLA-FDM parameters for enhancement of industrial product mechanical performance based on GRA-RSM and BBD", *Progress in Additive Manufacturing*, Vol. 10 No. 2, pp. 1355-1383.

Chinchanikar, S., Shinde, S., Gaikwad, V., Shaikh, A., Rondhe, M. and Naik, M. (2022), "ANN modelling of surface roughness of FDM parts considering the effect of hidden layers, neurons, and process parameters", *Advances in Materials and Processing Technologies*, Vol. 10 No. 1, pp. 1-11.

Chinchanikar, S., Shinde, S., Shaikh, A., Gaikwad, V. and Ambhore, N.H. (2024), "Multi-objective optimization of FDM using hybrid genetic algorithm-based multi-criteria decision-making (MCDM) techniques", *Journal of The Institution of Engineers (India): Series D*, Vol. 105 No. 1, pp. 49-63.

Deshwal, S., Kumar, A. and Chhabra, D. (2020), "Exercising hybrid statistical tools GA-RSM, GA-ANN and GA-ANFIS to optimize FDM process parameters for tensile strength improvement", *CIRP Journal of Manufacturing Science and Technology*, Vol. 31, pp. 189-199.

Dev, S. and Srivastava, R. (2023), "Influence of process variables on mechanical properties and material weight of acrylic butadiene styrene parts produced by fused filament fabrication", *Progress in Additive Manufacturing*, Vol. 8 No. 2, pp. 143-158.

Dey, A. and Yodo, N. (2019), "A systematic survey of FDM process parameter optimization and their influence on part characteristics", *Journal of Manufacturing and Materials Processing*, Vol. 3 No. 3, p. 64.

Dixit, M., Yadav, P. and Singhal, P. (2024), "Multi-objective parametric optimization of fused deposition additive manufacturing (FDAM) for prosthetic part", *Journal of The Institution of Engineers (India): Series C*, Vol. 105 No. 5, pp. 1165-1179.

Esakki, B., Ali, T.K., Rajamani, D. and Sachin, S. (2021), "Parametric optimization on impact strength of selective inhibition sintering fabricated PA-12 parts based on evolutionary optimization algorithms", *Journal of Materials Engineering and Performance*, Vol. 30 No. 7, pp. 5356-5663.

Fountas, N.A., Papantoniou, I., Kechagias, J.D., Manolakos, D.E. and Vaxevanidis, N.M. (2022), "Modeling and optimization of flexural properties of FDM-processed PET-G specimens using RSM and GWO algorithm", *Engineering Failure Analysis*, Vol. 138, p. 106340.

Gebisa, A.W. and Lemu, H.G. (2018), "Investigating effects of fused-deposition modeling (FDM) processing parameters on flexural properties of ULTEM 9085 using designed experiment", *Materials*, Vol. 11 No. 4, p. ma11040500.

Giri, J., Shahane, P., Jachak, S., Chadge, R. and Giri, P. (2021), "Optimization of FDM process parameters for dual

extruder 3d printer using artificial neural network", *Materials Today: Proceedings*, Vol. 43, pp. 3242-3249.

Gurrala, P.K. and Regalla, S.P. (2014), "Multi-objective optimisation of strength and volumetric shrinkage of FDM parts a multi-objective optimization scheme is used to optimize the strength and volumetric shrinkage of FDM parts considering different process parameters", *Virtual and Physical Prototyping*, Vol. 9 No. 2, pp. 127-138.

Kamaal, M., Anas, M., Rastogi, H., Bhardwaj, N. and Rahaman, A. (2021), "Effect of FDM process parameters on mechanical properties of 3D-printed carbon fibre-PLA composite", *Progress in Additive Manufacturing*, Vol. 6 No. 1, pp. 63-69.

Katoch, S., Chauhan, S.S. and Kumar, V. (2021), "A review on genetic algorithm: past, present, and future", *Multimed Tools Appl*, Vol. 80 No. 5, pp. 8091-8126.

Kumar, P., Gupta, P. and Singh, I. (2022), "Parametric optimization of FDM using the ANN-based whale optimization algorithm", *Ai Edam-Artificial Intelligence for Engineering Design Analysis and Manufacturing*, Vol. 36.

Meiabadi, M.S., Moradi, M., Karamimoghadam, M., Ardabili, S., Bodaghi, M., Shokri, M. and Mosavi, A.H. (2021), "Modeling the producibility of 3D printing in polylactic acid using artificial neural networks and fused filament fabrication", *Polymers (Basel)*, Vol. 13 No. 19, p. 3219.

Ngo, T.D., Kashani, A., Imbalzano, G., Nguyen, K.T.Q. and Hui, D. (2018), "Additive manufacturing (3D printing): a review of materials, methods, applications and challenges", *Composites Part B: Engineering*, Vol. 143, pp. 172-196.

Pazhamannil, R.V., Govindan, P. and Sooraj, P. (2021), "Prediction of the tensile strength of polylactic acid fused deposition models using artificial neural network technique", *Materials Today: Proceedings*, Vol. 46, pp. 9187-9193.

Pinho, L.A.G., Lima, A.L., Sa-Barreto, L.L., Gratieri, T., Gelfuso, G.M., Marreto, R.N. and Cunha-Filho, M. (2021), "Preformulation studies to guide the production of medicines by fused deposition modeling 3D printing", *AAPS PharmSciTech*, Vol. 22 No. 8, p. 263.

Pires, F.Q., Alves-Silva, I., Pinho, L.A.G., Chaker, J.A., Sa-Barreto, L.L., Gelfuso, G.M., Gratieri, T. and Cunha-Filho, M. (2020), "Predictive models of FDM 3D printing using experimental design based on pharmaceutical requirements for tablet production", *International Journal of Pharmaceutics*, Vol. 588, p. 119728.

Raju, M., Gupta, M.K., Bhanot, N. and Sharma, V.S. (2019), "A hybrid PSO-BFO evolutionary algorithm for optimization of fused deposition modelling process parameters", *Journal of Intelligent Manufacturing*, Vol. 30 No. 7, pp. 2743-2758.

Ramesh, M. and Panneerselvam, K. (2021), "Mechanical investigation and optimization of parameter selection for nylon material processed by FDM", *Materials Today: Proceedings*, Vol. 46, pp. 9303-9307.

Romero, P.E., Arribas-Barrios, J., Rodriguez-Alabanda, O., González-Merino, R. and Guerrero-Vaca, G. (2021), "Manufacture of polyurethane foam parts for automotive industry using FDM 3D printed molds", *CIRP Journal of Manufacturing Science and Technology*, Vol. 32, pp. 396-404.

Samykano, M., Selvamani, S.K., Kadirgama, K., Ngui, W.K., Kanagaraj, G. and Sudhakar, K. (2019), "Mechanical property of FDM printed ABS: influence of printing parameters", *The International Journal of Advanced Manufacturing Technology*, Vol. 102 Nos 9-12, pp. 2779-2796.

Shemelya, C., De La Rosa, A., Torrado, A.R., Yu, K., Domanowski, J., Bonacuse, P.J., Martin, R.E., Juhasz, M., Hurwitz, F., Wicker, R.B., Conner, B., MacDonald, E. and Roberson, D.A. (2017), "Anisotropy of thermal conductivity in 3D printed polymer matrix composites for space based cube satellites", *Additive Manufacturing*, Vol. 16, pp. 186-196.

Sieradzka, M., Fabia, J., Binias, D., Graczyk, T. and Fryczkowski, R. (2021), "High-impact polystyrene reinforced with reduced graphene oxide as a filament for fused filament fabrication 3D printing", *Materials*, Vol. 14 No. 22, p. 7008.

Singh, S., Singh, N., Gupta, M., Prakash, C. and Singh, R. (2019), "Mechanical feasibility of ABS/HIPS-based multi-material structures primed by low-cost polymer printer", *Rapid Prototyping Journal*, Vol. 25 No. 1, pp. 152-161.

Stanaitis, K., Čižas, V., Bielevičiūtė, A., Grigelionis, I. and Minkevičius, L. (2024), "High-impact polystyrene structured light components for terahertz imaging applications", *Sensors*, Vol. 25 No. 1, p. 131.

Tayyab, M., Ahmad, S., Akhtar, M.J., Sathikh, P.M. and Singari, R.M. (2023), "Prediction of mechanical properties for acrylonitrile-butadiene-styrene parts manufactured by fused deposition modelling using artificial neural network and genetic algorithm", *International Journal of Computer Integrated Manufacturing*, Vol. 36 No. 9, pp. 1295-1312.

Thuong, N.T., Lam, N.B., Son, P.A., Chien, N.B., Linh, N.P. D., Nam, C.T.H. and Vu, N.A. (2024), "Preparation and characterization of thermally conductive high impact polystyrene/AlN composite", *International Journal of Polymer Science*, Vol. 2024 No. 1, pp. 1-9.

Tura, A.D., Lemu, H.G., Mamo, H.B. and Santhosh, A.J. (2023), "Prediction of tensile strength in fused deposition modeling process using artificial neural network and fuzzy logic", *Progress in Additive Manufacturing*, Vol. 8 No. 3, pp. 529-539.

Vidakis, N., Petousis, M., Kourinou, M., Velidakis, E., Mountakis, N., Fischer-Griffiths, P.E., Grammatikos, S. and Tzounis, L. (2021), "Additive manufacturing of multifunctional polylactic acid (PLA)—multiwalled carbon nanotubes (MWCNTs) nanocomposites", *Nanocomposites*, Vol. 7 No. 1, pp. 184-199.

Vijayaraghavan, V., Garg, A., Lam, J.S.L., Panda, B. and Mahapatra, S.S. (2015), "Process characterisation of 3D-printed FDM components using improved evolutionary computational approach", *International Journal of Advanced Manufacturing Technology*, Vol. 78 Nos 5-8, pp. 781-793.

Wang, S.H., Ma, Y.B., Deng, Z.C., Zhang, S. and Cai, J.X. (2020), "Effects of fused deposition modeling process parameters on tensile, dynamic mechanical properties of 3D printed polylactic acid materials", *Polymer Testing*, Vol. 86, p. 106483.

Wankhede, V., Jagetiya, D., Joshi, A. and Chaudhari, R. (2020), "Experimental investigation of FDM process parameters using Taguchi analysis", *Materials Today: Proceedings*, Vol. 27, pp. 2117-2120.

Wu, J., Chen, X.-Y., Zhang, H., Xiong, L.-D., Lei, H. and Deng, S.-H. (2019), "Hyperparameter optimization for

machine learning models based on Bayesian optimization", *Journal of Electronic Science and Technology*, Vol. 17 No. 1, pp. 26-40.

Xu, Y., Unkovskiy, A., Klaue, F., Rupp, F., Geis-Gerstorfer, J. and Spintzyk, S. (2018), "Compatibility of a silicone impression/adhesive system to FDM-printed tray materials-A laboratory peel-off study", *Materials (Basel)*, Vol. 11 No. 10, p. 1905.

Yadav, D., Chhabra, D., Kumar Garg, R., Ahlawat, A. and Phogat, A. (2020), "Optimization of FDM 3D printing process parameters for multi-material using artificial neural network", *Materials Today: Proceedings*, Vol. 21, pp. 1583-1591.

Yan, Z., Guo, X., Hui, J., Lv, J. and Xu, Z. (2025), "Optimization of energy consumption and dimensional accuracy for fused deposition modeling processes through a hybrid method", *The International Journal of Advanced Manufacturing Technology*, Vol. 137 Nos 5-6.

Zaafarani, N.N., Nour, M., El-Kassas, A.M. and Elsheikh, A. (2024), "A new recycled high-impact polystyrene-rice straw composite: eco-friendly fabrication and characterization", *International Journal of Environmental Science and Technology*, Vol. 21 No. 2, pp. 1193-1202.

Zohdi, N. and Yang, R. (. (2021), "Material anisotropy in additively manufactured polymers and polymer composites: a review", *Polymers*, Vol. 13 No. 19, p. 3368.

Zohdi, N.T. and Yang, C. (2019), "Investigation on mechanical anisotropy of high impact polystyrene fabricated via fused deposition modelling", *Proceedings of the International Conference on Mechanical and Manufacturing Engineering Research and Practice*, pp. 24-28.

Corresponding author

Richard (Chunhui) Yang can be contacted at: r.yang@westernsydney.edu.au